


RESEARCH ARTICLE | *Central Pattern Generators*

The Kölliker-Fuse nucleus orchestrates the timing of expiratory abdominal nerve bursting

William H. Barnett,¹ Sarah E. M. Jenkin,² William K. Milsom,² Julian F. R. Paton,^{3,4}
Ana P. Abdala,^{3*}  Yaroslav I. Molkov,^{1,5*} and Daniel B. Zoccal^{6*}

¹Department of Mathematics and Statistics, Georgia State University, Atlanta, Georgia; ²Department of Zoology, University of British Columbia, Vancouver, British Columbia, Canada; ³School of Physiology, Pharmacology and Neuroscience, Faculty of Biomedical Sciences, University of Bristol, Bristol, United Kingdom; ⁴Department of Physiology, Faculty of Medical and Health Sciences, The University of Auckland, Auckland, New Zealand; ⁵Neuroscience Institute, Georgia State University, Atlanta, Georgia; and ⁶Department of Physiology and Pathology, São Paulo State University, Araraquara, Brazil

Submitted 5 July 2017; accepted in final form 25 October 2017

Barnett WH, Jenkin SE, Milsom WK, Paton JF, Abdala AP, Molkov YI, Zoccal DB. The Kölliker-Fuse nucleus orchestrates the timing of expiratory abdominal nerve bursting. *J Neurophysiol* 119: 401–412, 2018. First published October 25, 2017; doi:10.1152/jn.00499.2017.—Coordination of respiratory pump and valve muscle activity is essential for normal breathing. A hallmark respiratory response to hypercapnia and hypoxia is the emergence of active exhalation, characterized by abdominal muscle pumping during the late one-third of expiration (late-E phase). Late-E abdominal activity during hypercapnia has been attributed to the activation of expiratory neurons located within the parafacial respiratory group (pFRG). However, the mechanisms that control emergence of active exhalation, and its silencing in restful breathing, are not completely understood. We hypothesized that inputs from the Kölliker-Fuse nucleus (KF) control the emergence of late-E activity during hypercapnia. Previously, we reported that reversible inhibition of the KF reduced postinspiratory (post-I) motor output to laryngeal adductor muscles and brought forward the onset of hypercapnia-induced late-E abdominal activity. Here we explored the contribution of the KF for late-E abdominal recruitment during hypercapnia by pharmacologically disinhibiting the KF in in situ decerebrate arterially perfused rat preparations. These data were combined with previous results and incorporated into a computational model of the respiratory central pattern generator. Disinhibition of the KF through local parenchymal microinjections of gabazine (GABA_A receptor antagonist) prolonged vagal post-I activity and inhibited late-E abdominal output during hypercapnia. In silico, we reproduced this behavior and predicted a mechanism in which the KF provides excitatory drive to post-I inhibitory neurons, which in turn inhibit late-E neurons of the pFRG. Although the exact mechanism proposed by the model requires testing, our data confirm that the KF modulates the formation of late-E abdominal activity during hypercapnia.

NEW & NOTEWORTHY The pons is essential for the formation of the three-phase respiratory pattern, controlling the inspiratory-expiratory phase transition. We provide functional evidence of a novel role for the Kölliker-Fuse nucleus (KF) controlling the emergence of abdominal expiratory bursts during active expiration. A computational

model of the respiratory central pattern generator predicts a possible mechanism by which the KF interacts indirectly with the parafacial respiratory group and exerts an inhibitory effect on the expiratory conditional oscillator.

abdominal expiratory activity; active expiration; pons; respiratory pattern; ventral respiratory column

INTRODUCTION

Resting respiratory rhythmogenesis in mammals is suggested to emerge primarily from an inspiratory oscillator located in the medullary respiratory group, which contains neurons that are sufficient to produce rhythmic inspiratory activity in vitro (Anderson et al. 2016; Smith et al. 1991). However, generation of the functionally relevant respiratory rhythm and pattern seen in vivo requires interactions between the inspiratory oscillator and other respiratory regions (Smith et al. 2007). Accumulating evidence supports the notion that descending inputs from the pontine respiratory group, historically identified as the pneumotaxic center of the brain (Lumsden 1923), are important for generation of eupneic breathing. Within this region, the Kölliker-Fuse nucleus (KF) has been identified as an essential region to gate the postinspiratory (post-I) phase and control I-to-E phase transitions (Dutschmann and Dick 2012; Molkov et al. 2013; Mörschel and Dutschmann 2009). The KF contains neurons that provide mainly excitatory synaptic inputs to medullary respiratory regions (Ezure and Tanaka 2006; Geerling et al. 2017; Rosin et al. 2006). Ablation of the KF inputs prolongs inspiratory duration and produces apneusis (Bautista and Dutschmann 2014; Harris and Milsom 2003; Molkov et al. 2013; Morrison et al. 1994; St-John and Paton 2004), indicating a significant role of the KF neurons in breathing rhythm generation. Experimental evidence also highlights the role of the KF in the formation of the cranial respiratory motor activity that controls tongue and laryngeal musculature. Microinjection of excitatory amino acid agonists into the KF parenchyma promotes tonic excitation of post-I motor activity in the vagus/laryngeal recurrent nerve, increases laryngeal constrictor activity, prolongs expiratory phase dura-

* A. P. Abdala, Y. I. Molkov, and D. B. Zoccal contributed equally to this work.

Address for reprint requests and other correspondence: D. B. Zoccal, Dept. of Physiology and Pathology, School of Dentistry of Araraquara, São Paulo State Univ. (UNESP), Rua Humaitá, 1680, 14801-903 Araraquara, SP, Brazil (e-mail: zoccal@foar.unesp.br).

tion, and promotes swallowing-related resetting of the respiratory cycle (Abdala et al. 2016; Bonis et al. 2013; Dutschmann and Herbert 2006). In contrast, pharmacological inhibition of the KF eliminates the post-I component of vagus nerve activity, diminishes hypoglossal nerve and genioglossal activities, and reduces upper airway resistance (Dutschmann and Herbert 2006; Levitt et al. 2015; Silva et al. 2016a). These studies suggest that KF neurons also interact with the medullary premotor respiratory neurons that control upper airway patency during eupnea or oropharyngeal reflexes.

Under conditions of elevated metabolic demand, such as elevated partial pressure of CO₂ (hypercapnia) or low O₂ (hypoxia) in the blood, an active expiratory pattern emerges to support pulmonary hyperventilation (Jenkin and Milsom 2014; Lemes and Zoccal 2014). A distinct feature of active expiration is the generation of rhythmical bursts of abdominal expiratory activity during the late one-third of expiration (aka late-E or E2 phase) (Moraes et al. 2014; Pagliardini et al. 2011). In juvenile/adult animals, the generation of abdominal activity relies on the activation of neurons located in the parafacial respiratory group (pFRG), which are suggested to comprise a conditional expiratory oscillator (Abdala et al. 2009; Janczewski and Feldman 2006; Marina et al. 2010; Molkov et al. 2014). Under resting conditions (normoxia and eucapnia), it is suggested that the expiratory pFRG oscillator is synaptically suppressed (de Britto and Moraes 2017; Molkov et al. 2010; Pagliardini et al. 2011; Rubin et al. 2011). During hypercapnia or hypoxia, activation of central and peripheral chemoreceptors brings about rhythmic incrementing bursts in a subpopulation of pFRG neurons, which occur during the late third of the expiratory period (late-E) and correlate with contractions in abdominal expiratory muscles and active exhalation (Abbott et al. 2011; Abdala et al. 2009; Barnett et al. 2017; Marina et al. 2010; Molkov et al. 2011; Moraes et al. 2012; Silva et al. 2016b). Interestingly, peripheral and central chemoreceptors are suggested to provide tonic excitatory inputs to pontine-medullary respiratory neurons (de Britto and Moraes 2017; Mifflin 1990; Moreira et al. 2007), indicating that synaptic excitatory and inhibitory interactions between the pFRG expiratory oscillator and the respiratory central pattern generator (CPG) are necessary for abdominal pattern formation.

Experiments showing that ponto-medullary transection prevented the emergence of expiratory bursts in abdominal motor nerves during hypercapnia (Abdala et al. 2009) provide evidence for the involvement of the pons in the control of active expiratory motor activity. We recently verified that microinjections of a GABA_A receptor agonist into the KF parenchyma caused an earlier onset of hypercapnia-induced late-E abdominal activity (Jenkin et al. 2017). These data suggest an inhibitory influence of the KF neurons on the pFRG oscillator, regulating the timing of evoked expiratory bursts in abdominal activity in conditions of metabolic challenge. Although reciprocal connections have been found between the KF and the pFRG regions (Rosin et al. 2006; Silva et al. 2016a), it has been reported that the KF projections to ventromedullary neurons, including those activated during hypercapnia, are predominantly excitatory (Geerling et al. 2017; Yokota et al. 2015) and that local inhibitory neurons are sparse (Abdala et al. 2016; Guthmann et al. 1998). These experimental observations suggest that the inhibitory effects of KF neurons on the pFRG oscillator are indirect.

In light of these observations, in the present study we aimed to further investigate the inhibitory role of KF neurons in the generation of active abdominal expiratory activity. Specifically, we tested the prediction that artificially increased activity of KF neurons during hypercapnia would cause a suppression of evoked late-E abdominal motor output. The data obtained in this study combined with our previous experimental findings (Jenkin et al. 2017) were used to extend a previous computational model of the respiratory CPG (Molkov et al. 2010; Rybak et al. 2007), then generating a hypothetical model that could provide mechanistic insight on how the KF may interact with the respiratory circuitry in the medulla to control late-expiratory abdominal activity during hypercapnia.

METHODS

Experimental Data

Part of the data used here, which relate to pharmacological inhibition of the KF, was extracted from our recently published study (Jenkin et al. 2017) and was reanalyzed in the present study to be included in the model. The new experimental data presented here were collected as described below.

Animals

The experimental procedures complied with the guidelines of the National Institutes of Health (NIH Publication No. 85-23, 1996) and of the Brazilian National Council for Animal Experimentation Control (CONCEA), were performed according to the United Kingdom Home Office's Animals (Scientific Procedures) Act (1986), and were approved by the University of Bristol Animal Welfare and Ethical Review Body. Juvenile male Wistar rats ($n = 6$; P21–25, 50–60 g) were housed with free access to rat chow and water, under controlled conditions of temperature ($22 \pm 1^\circ\text{C}$), humidity (50–60%), and light-dark cycle (12:12 h, lights on at 7:00 AM).

In Situ Decerebrate Arterially Perfused Rats

In situ decerebrate arterially perfused rats (Paton 1996) were surgically prepared as previously described (Zoccal et al. 2008). Briefly, rats were heparinized (1,000 IU) and subsequently anesthetized deeply with halothane until the paw and tail pinch reflexes were abolished, transected below the diaphragm, and submerged in a cold Ringer solution (in mM: 125 NaCl, 24 NaHCO₃, 3.75 KCl, 2.5 CaCl₂, 1.25 MgSO₄, 1.25 KH₂PO₄, 10 dextrose). They were decerebrated (precollicularly), and the cerebellum was removed to expose the fourth ventricle and inferior colliculus. To measure inspiratory motor output, the lungs were removed and the left phrenic nerve was cut distally and recorded with a bipolar suction electrode. To measure motor output to laryngeal abductor and adductor muscles, the left vagus nerve (cVN) was isolated and cut at the cervical level (below the bifurcation of the common carotid artery). To measure output to abdominal muscles, nerves from the right lumbar plexus at thoracic-lumbar level (T₁₂–L₁) were dissected and cut distally and are referred to as abdominal nerve (AbN). Preparations were then transferred to a recording chamber; the descending aorta was cannulated and perfused retrogradely (21–24 ml/min; Watson-Marlow 502s, Falmouth, UK) via a double-lumen cannula with Ringer solution containing 1.25% polyethylene glycol (an oncotic agent; Sigma, St. Louis, MO) and vecuronium bromide (a neuromuscular blocker; 3–4 μg/ml). The perfusion pressure was held within 55–75 mmHg by addition of vasopressin (0.5 nM; Sigma) to the perfusate. The perfusate was continuously gassed with 5% CO₂-95% O₂ (pH 7.4), warmed to 31–32°C, and filtered with a nylon mesh (25 μm). Arterial perfusion pressure was recorded with a Gould transducer and amplifier (series

6600). Bioelectric signals were amplified (10,000 \times), band-pass filtered (0.3–5 kHz) (AC Amplifier model 1700, A-M Systems, Sequim, WA), and recorded with an ADC signal conditioner (10 kHz; Micro1401, Cambridge Electronic Design, Cambridge, UK).

Brain Stem Microinjections

Microinjections were performed with custom-made, three-barrel glass micropipettes (borosilicate, OD 1.5 mm, ID 0.86 mm; Harvard Apparatus) filled with L-glutamate (10 mM; Sigma-Aldrich), gabazine (a GABA_A receptor antagonist, 0.1–1 mM; Sigma-Aldrich), and 2% Evans blue dye (Sigma-Aldrich). All drugs were dissolved in artificial cerebrospinal fluid and adjusted to pH 7.4 when needed. The micropipette tips were positioned 0.3–0.5 caudal to the inferior colliculus, 1.9–2.1 mm from the midline, and 1–1.5 mm of the dorsal surface, as previously described (Abdala et al. 2016). Location of the microinjections was aided with the use of a surgical binocular microscope, and the injection volumes (60 nl) were controlled with a precalibrated eyepiece reticule. The right and left KF were functionally identified with unilateral glutamate microinjections, which evoked phrenic nerve (PN) burst inhibition and prolonged cVN post-I activity (Dutschmann and Herbert 2006). The left- and right-side identifications were performed in random order, and a time interval of 5 min was allowed between consecutive glutamate microinjections. After a recovery period of at least 10 min, the KF was pharmacologically disinhibited bilaterally through microinjections of gabazine (Mandel and Schreier 2009). The contralateral injection of gabazine was always performed within 1–2 min of the first injection. After the experiments, microinjection sites were marked with Evans blue dye and verified histologically post hoc. Brain stems were removed and fixed in 4% paraformaldehyde, cryoprotected in 30% sucrose overnight, and sectioned in a freezing microtome (40 μ m). Sections were Nissl counterstained (2% Neutral Red) and mounted with DPX (Sigma-Aldrich). Microinjection sites were photographed and documented on schematic outlines of the dorsolateral pons (Paxinos and Watson 2007).

Hypercapnic Stimulus

After stabilization and initial baseline recordings, in situ preparations were exposed to hypercapnia by raising the fractional concentration of CO₂ in the perfusate from 5% to 8–10% (balanced with O₂) for 5 min to generate active expiration (Abdala et al. 2009; Molkov et al. 2011). The effects peaked and reached steady state after 3 min of exposure. The stimulus was applied before and after bilateral microinjections of gabazine into the KF.

Data Analyses

Analyses were performed on rectified and smoothed signals (time constant of 50 ms) with custom-written subroutines in Spike 7.10 software (Cambridge Electronic Design). PN burst frequency was calculated in cycles per minute (cpm). The coefficient of variation (CoV) of PN burst frequency was calculated as an indicator of respiratory cycle variability. The duration of the cVN postinspiratory component (decrementing activity during the expiratory phase) was expressed as a percentage of total expiratory time (i.e., inter-PN burst interval). To quantify AbN activity during eupnea, each individual expiratory cycle was divided into its initial two-thirds, which was dominated by the post-I phase (also known as E1), and the final one-third, which predominantly corresponded to the late-E phase (also known as E2). The maximum amplitudes above baseline of AbN output occurring during the first two-thirds and late one-third of each individual expiratory cycle were measured and averaged over 15–25 cycles (1-min epoch) and expressed in microvolts. As described previously by Abdala et al. (2009), high-amplitude incrementing AbN bursts during the final one-third of expiration, referred to as AbN

late-E bursts, only emerge in conditions of hypercapnia and/or hypoxia, and displayed quantal skipping in relation to PN cycles. To quantify these, a threshold crossing was defined, which was typically set at 75% of the maximum amplitude of AbN activity during the final one-third of expiration under a hypercapnia challenge. As previously described (Abdala et al. 2009), in order to accommodate it, the occurrence of a high-amplitude AbN late-E burst in a given cycle during hypercapnia coincides with a truncated cVN post-I cycle. To quantify this phenomenon during hypercapnia, we subtracted the length of post-I cycles without AbN late-E bursts (nontruncated) from cycles with late-E bursts (truncated), and this is referred to as post-I truncation expressed as Δ Pit (ms).

All results are reported as means \pm SE. The normal distribution of the data was verified with a D'Agostino and Pearson normality test, and comparisons were performed by paired nonparametric Wilcoxon *t*-test. GraphPad Prism (version 6) was used for statistical analyses, and differences were considered significant when $P < 0.05$.

Computational Methods

The model presented here is an extension of a previous model, which described sensitization of central chemoreceptors (Molkov et al. 2011). The Molkov et al. (2011) work drew from Molkov et al. (2010), which investigated the recruitment of the late expiratory oscillator in the pFRG for active expiration. Both models incorporate the network architecture of previous models (Rybak et al. 2007; Smith et al. 2007) inspired by ultraprecise pontine and medullary transection studies. As in our previous models, the respiratory neurons were classified according to their firing pattern (augmenting or decrementing) and phase (inspiratory or expiratory) relative to the phrenic cycle, as recorded experimentally (Abdala et al. 2009; Orem and Trotter 1992; Paton 1996; Rybak et al. 1997): early-inspiratory (early-I); ramping inspiratory (ramp-I); preinspiratory (pre-I); postinspiratory (post-I), augmenting expiratory (aug-E), and late-expiratory (late-E) neurons. Neuronal populations were composed of either 20 or 50 single-compartment neuron models described in the Hodgkin-Huxley formalism. Synaptic projections from one population to another were all to all, and excitatory projections from drive elements synapsed onto every postsynaptic neuron. The motoneuron output (PN, vagus nerve, and AbN) was computed by integrating the excitatory inputs. The connectivity of this model is detailed in Table 1.

Distinction from Previous Models

In contrast to previous models, a hyperpolarization-activated cationic current (I_h) was included in the post-I (e) (Böttinger complex, BötC) population to facilitate adaptation in the post-I component of the cVN motoneuron output. This current followed the Hodgkin-Huxley formalism; its contribution to the current-balance equation was $I_h = \bar{g}_h m_h (V - E_h)$, where V is the membrane potential, m_h is the activation variable, and the expression $\bar{g}_h m_h$ determines the instantaneous conductance of the current. The values of its biophysical parameters were adapted from the description in McCormick and Pape (1990). The maximal conductance (\bar{g}_h) was 2 nS, and the reversal potential (E_h) was -43 mV. The activation of I_h was determined by the equation

$$\frac{dm_h}{dt} = \frac{f(V) - m_h}{\tau(V)}$$

where the functions for steady-state activation $f(V)$ and time constant $\tau(V)$ take the following form:

$$f(V) = [1 + \exp([V + 60]/5.5)]^{-1}$$

and

$$\tau(V) = 1,500 / \cosh([V + 80]/13) \text{ ms}$$

Table 1. Detailed connectivity of computational model

Target Population	Excitatory Drive [weight of synaptic input] or Presynaptic Source Population [weight of synaptic input from single neuron]
aug-E (BötC)	Drive (Pons) [0.42]*, Drive (RTN) [2.3]†, early-I (1) (pre-BötC) [-0.135], late-E (pFRG) [0.03]†, post-I (BötC) [-0.3]
early-I (1) (pre-BötC)	Drive (RTN) [2]*, Drive (KF) [0.6]†§, aug-E (BötC) [-0.265], post-I (BötC) [-0.45], pre-I (pre-BötC) [0.05]*
early-I (2) (rVRG)	Drive (Pons) [2.5], aug-E (BötC) [-0.25], post-I (BötC) [-0.5]
late-E (pFRG)	Drive (RTN) [0.225, 0.325]*‡, early-I (1) (pre-BötC) [-0.05]*, late-E (pFRG) [0.024]*, post-I (BötC) [-0.0275]*, pre-I (pre-BötC) [0.013]†
post-I (BötC)	Drive (Pons) [1]*, Drive (KF) [0.65]†§, early-I (1) (pre-BötC) [-0.025]
post-I (e) (BötC)	Drive (Pons) [0.8]*, aug-E (BötC) [-0.3]*, early-I (1) (pre-BötC) [-0.2]*
pre-I (pre-BötC)	Drive (RTN) [0.198, 0.286]‡, Drive (Pons) [0.65], Drive (Raphe) [0.15]*, aug-E (BötC) [-0.01]*, post-I (BötC) [-0.19]*, pre-I (pre-BötC) [0.02]*
ramp-I (rVRG)	Drive (Pons) [2], aug-E (BötC) [-0.1], early-I (2) (rVRG) [-0.3], post-I (BötC) [-2], pre-I (pre-BötC) [0.12]

*Value different from Molkov et al. (2011). †Not present in Molkov et al. (2011). ‡Drive (RTN) [eucapnia, hypercapnia]. §Isoguvacine and gabazine.

Numerical simulations were performed with NSM 3.0 software, which was developed by S. Markin, I. Rybak, and N. Shevtsova at Drexel University (Rybak et al. 2004, 2007). It was extended to use OpenMPI for high-performance computing clusters by Y. Molkov (Molkov et al. 2011). Solutions to ordinary differential equations were computed by the exponential Euler method for integration with a time step of 0.1 ms.

Model Adjustments

The response to hypercapnia in the model is mediated by an increase in a tonic drive attributed to chemosensitive neurons in the retrotrapezoid nucleus (RTN). The targets of this drive are the pFRG late-E population and the preinspiratory/inspiratory (pre-I/I) population of the pre-Bötzing complex (pre-BötC). The latter population, in turn, could also excite late-E populations in the pFRG and contribute to the generation of late-E activity (Barnett et al. 2017). The gain of this drive with changing CO₂ was set to support late expiratory activity in the late-E population of the pFRG. We also considered that, for pattern formation, pFRG late-E neurons receive phasic inhibition during early inspiration and postinspiration from the respiratory CPG (Abdala et al. 2009; Molkov et al. 2010; Rubin et al. 2011), which in turn is excited by a tonic drive from the pons (Rybak et al. 2007; Smith et al. 2007).

Anatomical (Gang et al. 1995) and electrophysiological (Ezure and Tanaka 2006) studies indicate the existence of synaptic projections from the KF to the BötC region. In light of these observations, and studies showing that the majority of projections from the KF to lower brain stem respiratory groups are glutamatergic (Geerling et al. 2017), we proposed that an inhibitory post-I population of BötC neurons are under direct control by a KF population, which we model as a tonic excitatory drive (highlighted in Fig. 1). Under eupneic conditions, the KF-driven post-I population of the BötC inhibits both the RTN/pFRG expiratory population and the pre-I/I population. This inhibition suppresses late expiratory activity in the RTN/pFRG and contributes to the timing of the onset of inspiration (Fig. 1). Our data (this study and Jenkin et al. 2017) demonstrate that mild inhibition and disinhibition of the KF nucleus modulates the emergence of late-E activity during hypercapnia, without significantly disrupting eupneic respiration. Thus we reasoned that drive from the KF should also be distributed among both inspiratory and expiratory populations (Fig. 1) and inhibition or disinhibition of the KF nucleus should result in relatively balanced changes in drive to inspiratory and expiratory populations of the respiratory CPG. In previous iterations of the model (Barnett et al. 2017; Molkov et al. 2010), a component of the tonic drive to the early-I population of the pre-BötC was attributed to the pontine nuclei. Therefore, in the model of the present study we attributed a portion of the pontine drive received by the early-I population of the pre-BötC to the KF (highlighted in Fig. 1). For the purposes of simulation, inhibition of the KF was interpreted as a decrease in the excitatory

drive by 35% and disinhibition of the KF was interpreted as an increase in the excitatory drive by 30%. These percentage changes in excitatory conductance of the neurons receiving the KF drive were the values that best reproduced our experimental data. The remaining pontine drive was separate and independent from the KF drive and was invariant during increases or decreases to the KF drive.

We also adjusted network topology to promote preinspiratory and late-E activity that is distinct in time from inspiratory activity. In Molkov et al. (2010) and Molkov et al. (2011), the late-E pFRG population stimulated the pre-I/I population. This projection promoted entrainment of pre-I/I activity to the pFRG expiratory oscillator. In Barnett et al. (2017), an excitatory projection from the pre-I/I population to the late-E (pFRG) population was included so that an increased excitability of the pre-I/I population could lower the threshold for emergence of late-expiratory activity. Here we removed the

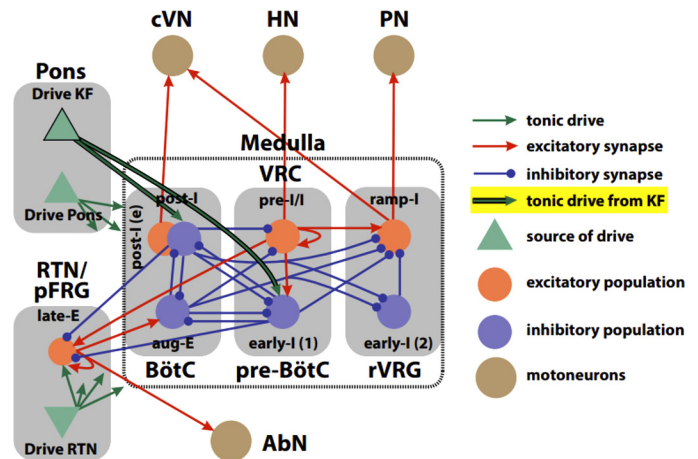


Fig. 1. Schematic of the brain stem respiratory network model including the inhibitory postinspiratory (post-I), excitatory postinspiratory [post-I(e)], and augmenting expiratory (aug-E) populations of the Bötzing complex (BötC); the preinspiratory/inspiratory (pre-I/I) and early-inspiratory [early-I (1)] populations of the pre-Bötzing complex (pre-BötC); the ramping inspiratory (ramp-I) and early-inspiratory [early-I (2)] populations of the rostral ventral respiratory group (rVRG); and the late-expiratory (late-E) population of the parafacial respiratory group (pFRG). This model includes excitatory drive elements, which are not modeled as populations and provide constant excitation to postsynaptic populations: drive from the pontine nuclei (Drive Pons), drive specifically from the Kölliker-Fuse nucleus (Drive KF), and drive from the retrotrapezoid nucleus (Drive RTN). Excitatory and inhibitory populations of 20–50 neurons are depicted as orange and blue elements, respectively. Similarly, projections from excitatory and inhibitory populations are colored orange and blue, respectively. Drive elements and projections associated with these elements are represented as green triangles or green arrows. The new additions to this model—Drive KF and its projections—are emphasized with black outline.

excitatory projection from the late-E (pFRG) population to the pre-I/I population. Excitation from the pre-I/I to the early-I population of the pre-BötC was diminished, and a component of the phasic excitation to the early-I population was replaced by a tonic drive, which is sufficient to support an inspiratory burst at the termination of expiration. We also incorporated an excitatory projection from the late-E pFRG expiratory population into the respiratory CPG that excited the aug-E population of the BötC. In the event of a burst in the RTN/pFRG expiratory oscillator, increased input to aug-E serves to prevent inspiratory burst initiation during the late-E burst in the pFRG, in agreement with previous experimental observations (Abdala et al. 2009).

RESULTS

Anatomical and Functional Identification of Microinjection Sites in KF

Unilateral microinjections of glutamate in the KF increased post-I activity in the cVN, prolonged expiratory time, and reduced PN burst frequency, as illustrated in Fig. 2A. Stimulation of the KF with glutamate did not alter the magnitude of resting AbN activity (Fig. 2A). Post hoc histological analyses confirmed that the microinjection sites were in the boundaries of the KF (Fig. 2B), between -8.64

and -8.88 mm in relation to bregma (Fig. 2C) (Paxinos and Watson 2007).

Baseline Respiratory Changes After Disinhibition of KF

Under resting conditions (eucapnia), the PN burst showed a ramping pattern of discharge, the cVN presented an inspiratory component (coincident with the PN burst) followed by post-I decrementing activity, and the AbN exhibited low-amplitude activity (relative to hypercapnia) during the expiratory phase, which was typically decrementing during the first two-thirds of expiration. One preparation also had low-amplitude incrementing AbN activity during the final one-third of expiration. Bilateral microinjections of low doses of gabazine in the KF caused a small but significant increase in the duration of post-I activity in the cVN ($68 \pm 7\%$ vs. $59 \pm 6\%$ of expiratory time, $P < 0.05$; Fig. 3, A and B). This effect was accompanied by an increase in PN burst frequency variability (CoV: 0.36 ± 0.10 vs. 0.15 ± 0.04 , $P < 0.05$; Fig. 3C), with no changes in PN burst frequency (23 ± 4 vs. 21 ± 4 cpm; Fig. 3D), time of inspiration (0.662 ± 0.05 vs. 0.757 ± 0.085 s), and time of expiration (2.72 ± 0.41 vs. 2.96 ± 1.02 s). Baseline mean AbN activity (3.81 ± 0.72 vs. 3.96 ± 0.71 μ V; Fig. 3E) did not change after gabazine microinjections in the KF.

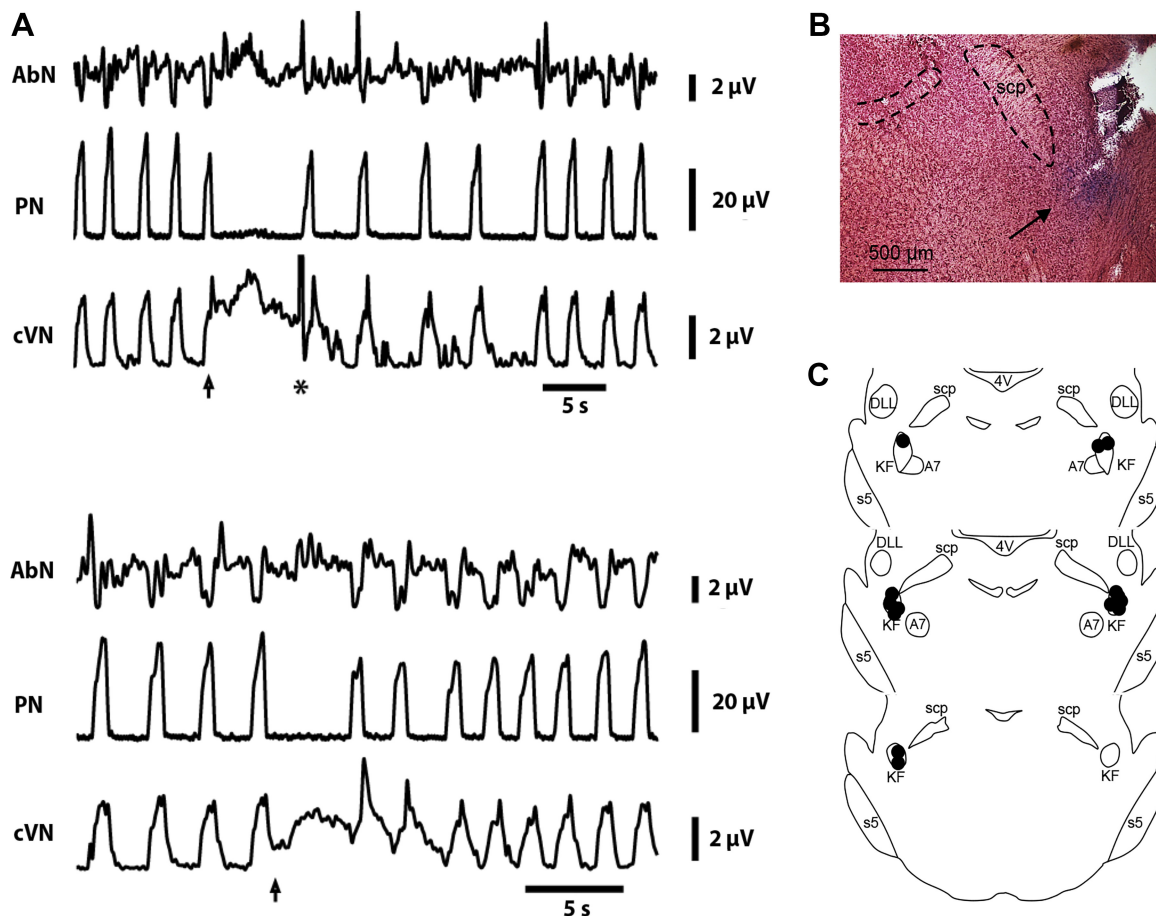


Fig. 2. Functional and histological identification of the Kölliker-Fuse nucleus (KF). A: integrated recordings of abdominal (AbN), phrenic (PN), and cervical vagus (cVN) nerve activities from an in situ rat preparation, representative of the group, illustrating the respiratory responses to microinjections of glutamate (arrow) in the left (top) and right (bottom) sides of the KF. *represents an artifact generated during the removal of the injection micropipette. B: photomicrograph of coronal section from the brain stem of a representative in situ rat preparation, illustrating the site of microinjection in the KF (arrow). C: schematic representations of all microinjection sites (black circles) into the KF ($n = 6$ each side). A7, A7 catecholaminergic cell group; DLL, dorsal nucleus of the lateral lemniscus; scp, superior cerebellar peduncle; s5, sensory root of trigeminal nerve; 4V, fourth ventricle.

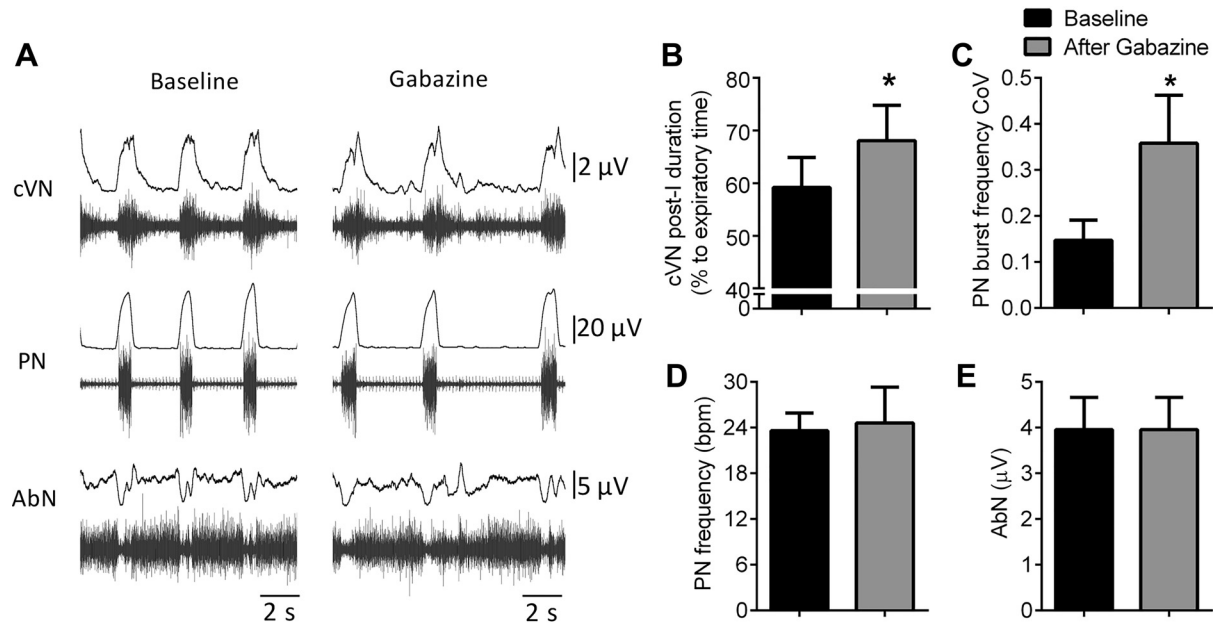


Fig. 3. Changes in baseline activities after microinjections of gabazine in the Kölliker-Fuse nucleus (KF). *A*: raw and integrated recordings of cervical vagus (cVN), phrenic (PN) and abdominal (AbN) nerve activities from a representative in situ rat preparation, illustrating the respiratory pattern before and after gabazine microinjections in the KF. *B–E*: average values of cVN post-I duration (normalized by expiratory time), coefficient of variation of PN burst frequency, mean PN burst frequency, and mean abdominal activity, respectively, before and after gabazine microinjections in the KF. *Different from baseline, $P < 0.05$. $n = 6$.

Effect of Disinhibition of KF on Generation of Late-E Bursts During Hypercapnia

With the increase in the fractional concentration of CO₂ in the perfusate (8–10%), late-E bursts emerged in AbN activity (Fig. 4) at a relative frequency ratio of 1:2 with the PN burst (Fig. 4, *A–C*) and 1:1 with the PN frequency at 10% CO₂ (Fig. 4, *D* and *E*). Concomitantly, post-I duration in the cVN was

reduced significantly (Fig. 5, *A* and *D*). No significant changes were observed in PN frequency during steady-state hypercapnia. After disinhibition of the KF, the magnitude of the AbN late-E response to hypercapnia was markedly suppressed (Fig. 4, *F–H*; Fig. 5*B*) (Δ : 8.2 ± 0.7 vs. $1.8 \pm 0.9 \mu\text{V}$ before and after gabazine, respectively, $P < 0.05$; Fig. 5*C*). This lower amplitude of AbN late-E bursts after gabazine microinjections

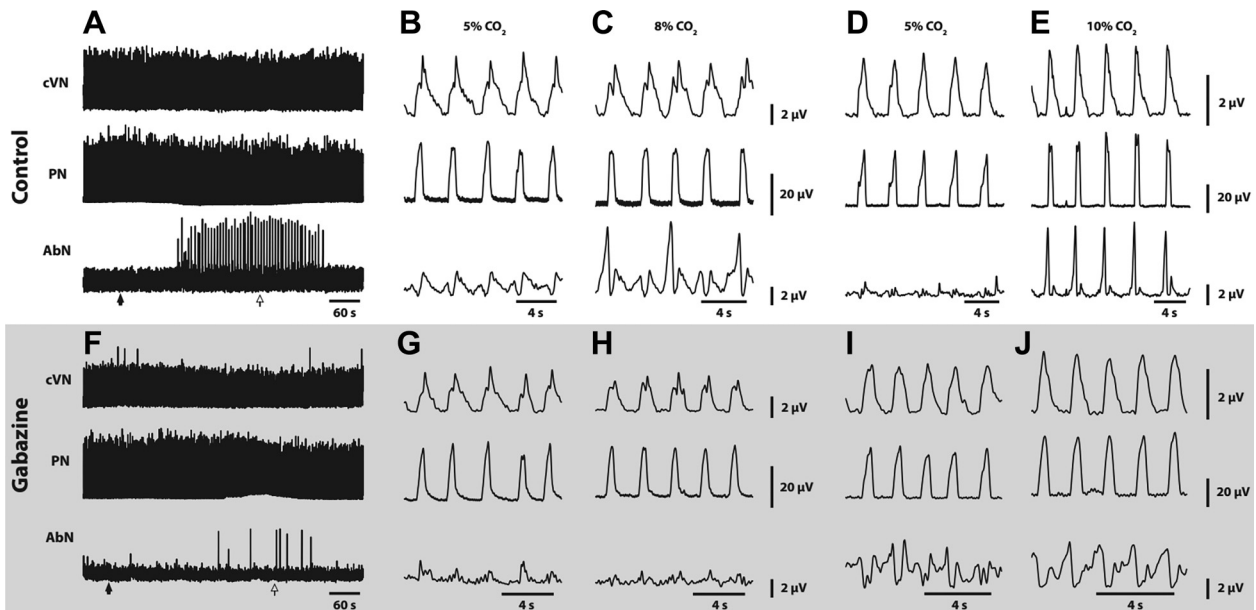


Fig. 4. Disinhibition of the Kölliker-Fuse nucleus suppresses the generation of abdominal late-E activity during hypercapnia. Recordings, from representative in situ rat preparations, depict the activity of central vagus nerve (cVN), phrenic nerve (PN), and abdominal nerve (AbN) in eucapnia and hypercapnia, before treatment (*A–E*) and after gabazine microinjections (*F–J*). All recordings performed after gabazine microinjections are indicated in the light gray box. Filled arrows and open arrows in *A* and *F* indicate the beginning and end of the change in perfusate CO₂ fractional concentration from 5% to 8%, respectively. Zoomed-in traces *B*, *D*, *G*, and *I* depict respective preceding eucapnia epochs; *C* and *H* depict 8% hypercapnia; and *E* and *J* depict 10% hypercapnia. *A–C* and *F–H* are from a preparation challenged with 8% CO₂. *D*, *E*, *I*, and *J* come from a separate preparation that was challenged with 10% CO₂.

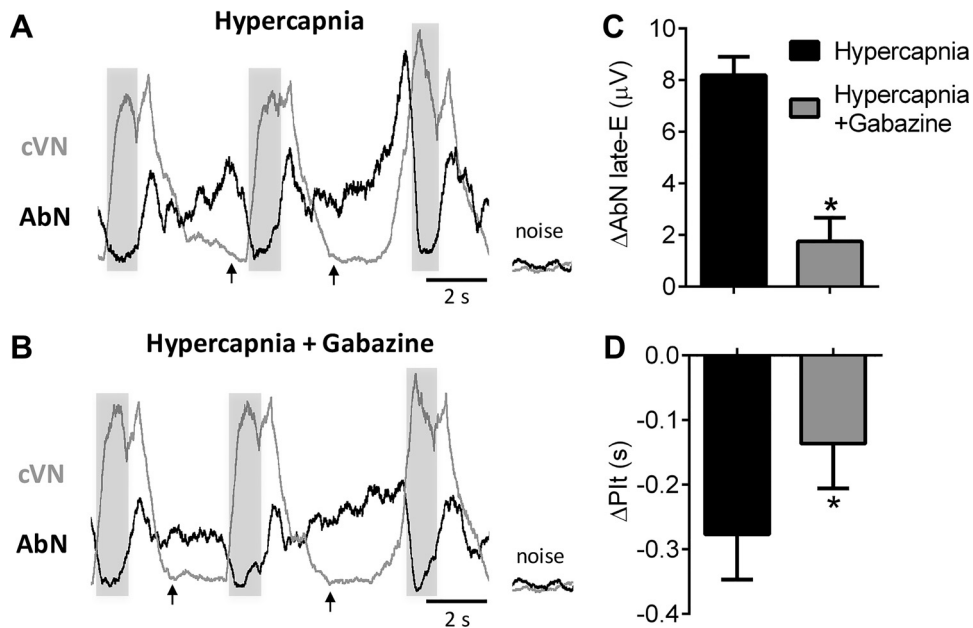


Fig. 5. Disinhibition of the Kölliker-Fuse nucleus (KF) prevented the reduction in vagal postinspiratory activity and restrained the generation of late-E abdominal activity during hypercapnia. *A* and *B*: superimposed traces of integrated cervical vagus (cVN, gray) and abdominal nerve (AbN, black) activities during hypercapnia from a representative in situ rat preparation, before and after gabazine microinjections in the KF. Gray box indicates the inspiratory phase (coincident with phrenic burst), and arrows indicate the end of postinspiratory (post-I) activity in cVN. Note that before gabazine microinjections the onset of the late-E burst in AbN during hypercapnia is associated with a clear truncation in post-I activity. After gabazine microinjections, the amplitude of AbN late-E burst reduced and post-I cVN activity presented minor changes. *C* and *D*: average values of AbN late-E burst amplitude and variation of cVN post-I duration during hypercapnia, before and after gabazine microinjections in the KF. *Statistically significantly different from baseline, $P < 0.05$. $n = 6$.

was associated with a reduced cVN post-I truncation (ΔPIt : -0.276 ± 0.070 vs. -0.137 ± 0.069 s before and after gabazine microinjections, respectively, $P < 0.05$; Fig. 5*D*). No significant changes were noted in the PN frequency during steady-state hypercapnia before vs. after gabazine microinjections in the KF (Δ : 2 ± 1 vs. 4 ± 2 cpm, respectively). Sixty minutes after gabazine microinjections, the magnitude of late-E bursts in AbN (Δ : 5.5 ± 0.6 μV) and the cVN post-I truncation (ΔPIt : -0.551 ± 0.147 s) evoked by hypercapnia were equivalent to pretreatment values.

Proposed Mechanisms Through Model Adjustments

We performed a series of computational experiments aimed at proposing a model that explains the changes to late-E activity in the AbN pattern during active expiration obtained in both this study and our previous related study (Jenkin et al. 2017). Based on the sum of the data, we identified the following key features of the motoneuron output during hypercapnia after pharmacological manipulation of the KF: 1) microinjections of isoguvacine (GABA_A receptor agonist) to inhibit the KF during hypercapnia suppressed the post-I component of the cVN and advanced the onset of late-E activity in the AbN, increasing its burst duration (Jenkin et al. 2017); 2) disinhibition of the KF during hypercapnia attenuated the shortening in post-I activity of cVN and reduced AbN late-E activity (present study). Our model was adjusted to reproduce these findings, as described in *Model Adjustments*.

Model Validation

Transient activation of KF drive in the model induces apnea. Application of glutamate in the KF evokes respiratory apnea during which there is increased post-I activity in the vagus nerve (Fig. 3). We reproduced these results by transiently increasing the KF drive by a factor of 4 (Fig. 6). Post-I (BötC) activity increased in amplitude and became tonic for the duration of the stimulation period; this population strongly inhibited aug-E (BötC) neuron activity. The excitatory premotor post-I (e) (BötC) population is responsible for the postin-

spiratory component of cVN, and it receives strong inhibition from aug-E (BötC) neurons. During the epoch of increased drive from the KF, post-I (e) (BötC) activity was disinhibited since aug-E (BötC) neurons did not fire; hence the activity in the cVN persisted for the duration of the excess KF input.

Suppression of KF drive enhances inspiratory phase duration. Previous studies have reported that inhibition of KF neurons reduces postinspiratory vagal activity and enhances inspiratory phase duration but does not modify baseline abdominal activity (Bautista and Dutschmann 2014, 2016; Jenkin et al. 2017). Our model simulations, which compared the activity of pre-BötC, BötC, and pFRG populations in eucapnia before (Fig. 7*A*) and after (Fig. 7*B*) KF inhibition, agree with these previous experimental observations. KF inhibition in eucapnia reduced the overall firing rate of the post-I (BötC) populations (inhibitory and excitatory) and increased the phase duration and firing frequency of the pre-I/I (pre-BötC) population (Fig. 7*B*) compared with the control simulation (Fig.



Fig. 6. Simulation of the glutamate microinjection into the Kölliker-Fuse nucleus (KF) by transient increase in drive from the KF to the respiratory CPG (arrow). Figure shows the activity of the phrenic nerve (PN) and the central vagus nerve (cVN) as well as the inhibitory postsynaptic (post-I), excitatory postsynaptic [post-I (e)], and augmenting-expiratory (aug-E) populations of the Bötzinger complex (BötC).

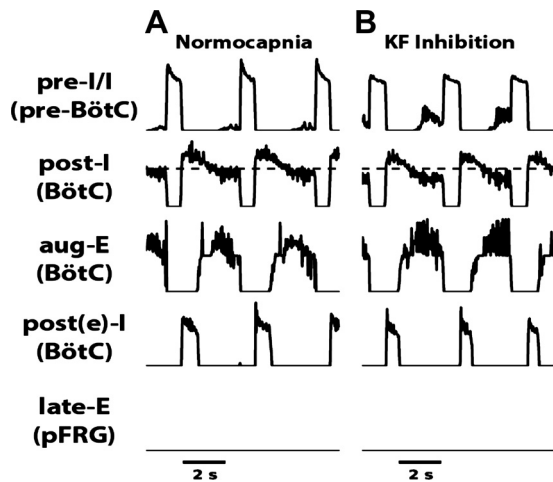


Fig. 7. Simulation of the Kölliker-Fuse nucleus (KF) inhibition in eucapnia. Model activity of central pattern generator populations under eucapnia (A) and KF inhibition (B). Figure shows the activities of the preinspiratory/inspiratory (pre-I/I) population of the pre-Bötzinger complex (pre-BötC); the inhibitory postinspiratory (post-I), augmenting expiratory (aug-E), and excitatory postinspiratory [post-I (e)] populations of the Bötzinger complex (BötC); and the late-expiratory (late-E) population of the pFRG. Horizontal dashed line emphasizes the change in amplitude of the inhibitory post-I population between A and B.

7A). Also, KF inhibition did not modify the activity of the late-E (pFRG) population.

Role of KF drive and pre-I excitation in active expiration. In our previous models, the emergence of active expiration during hypercapnia was dependent on an increase in the chemosensory drive from the RTN (Molkov et al. 2010, 2011). The same mechanism was implemented in this model. However, the late-E (pFRG) population also received increased excitatory input from the pre-I/I (pre-BötC) population during the E2 phase. To investigate the role of pre-I/I (pre-BötC) activity in the emergence and modulation of active expiration, we performed simulations in eucapnia (control simulation; Fig. 7A) and eucapnia with KF inhibition (Fig. 7B). KF inhibition in eucapnia reduced the overall firing rate of the post-I (BötC) population and increased the phase duration and firing frequency of the pre-I/I (pre-BötC) population (Fig. 7B) compared with the control simulation (Fig. 7A). Pharmacological disinhibition of the RTN/pFRG was shown to be sufficient to evoke late-E activity (Molkov et al. 2010; Pagliardini et al. 2011). However, in Jenkin et al. (2017), application of isoguvacine to the KF during eucapnia failed to evoke active expiration. Consistently, in these modeling results, reduction of the KF drive to post-I (BötC) populations created a combination of weak expiratory disinhibition and weak expiratory excitation, which was not sufficient to evoke late-E activity in accordance with the isoguvacine experiments during eucapnia.

Model Performance

Suppression of KF drive increases AbN late-E burst duration by reducing post-I inhibition. We implemented a pharmacological inhibition of the KF with isoguvacine in our extended model to explain the change in motoneuron output observed in our previous experimental results (Jenkin et al. 2017). This was simulated by a decrease in the tonic KF drive to the post-I (BötC) and early-I (pre-BötC) populations, and we refer to this manipulation in simulation as inhibition of the KF. Our anal-

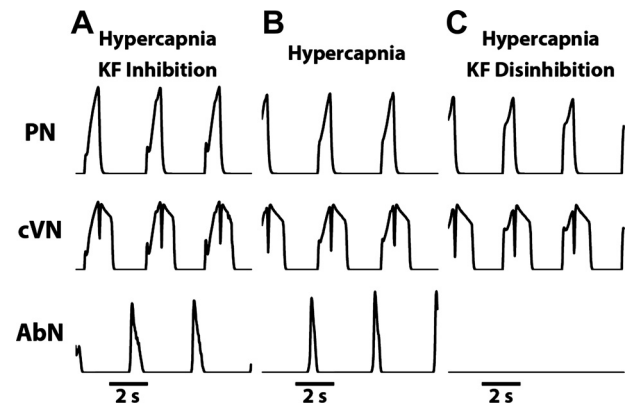


Fig. 8. Simulation of the Kölliker-Fuse nucleus (KF) inhibition and disinhibition in hypercapnia: motoneuron output in the model under hypercapnia + KF inhibition (A), hypercapnia (B), and hypercapnia + KF excitation (C), each depicting activity of the phrenic nerve (PN), the central vagus nerve (cVN), and the abdominal nerve (AbN).

ysis also included a simulation of hypercapnia with reduced KF drive (motoneuron output in Fig. 8A; CPG activity in Fig. 9A) and a simulation of the control condition—hypercapnia only (motoneuron output in Fig. 8B; CPG activity in Fig. 9B). Similar to the rat experiments with isoguvacine, a partial decrease in the KF drive during hypercapnia did not disrupt the three-phase respiratory rhythm in the model. Also, the model reproduced the advanced onset and increased phase duration of the AbN late-E burst in hypercapnia with reduced KF drive (Fig. 8A) as compared with hypercapnia with no additional manipulation to the KF (Fig. 8B).

In this model, the post-I (BötC) population fires in a decrementing fashion through the duration of expiration (Fig. 9) and is a main source of expiratory inhibition in the respiratory cycle. The late-E (pFRG) population receives both expiratory

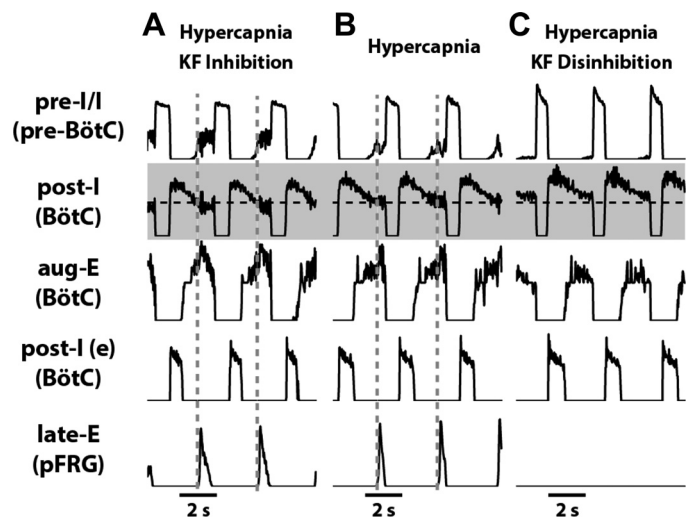


Fig. 9. Simulation of the Kölliker-Fuse nucleus (KF) inhibition and disinhibition in hypercapnia: model activity of central pattern generator populations under hypercapnia + KF inhibition (A), hypercapnia (B), and hypercapnia + KF excitation (C). post-I (BötC) traces are shaded gray for emphasis. Horizontal dashed black line in post-I (BötC) traces indicates the approximate threshold for activation of the late-E (pFRG). Vertical dashed gray lines indicate the phase of activation of late-E (pFRG). The included populations are the preinspiratory/inspiratory (pre-I/I) population of the pre-Bötzinger complex (pre-BötC); the inhibitory postinspiratory (post-I), augmenting expiratory (aug-E), and excitatory postinspiratory [post-I (e)] populations of the Bötzinger complex (BötC); and the late-expiratory (late-E) population of the pFRG.

and inspiratory inhibition in eucapnia (Fig. 1). During hypercapnia, the increase in tonic chemosensitive drive from the RTN lowers its threshold for activation. As the firing rate of the post-I (BötC) population decrements to a critical value, inhibition of late-E (pFRG) neurons decreases such that the population fires at the end of expiration (Fig. 9B). In the simulation including both reduced KF drive and hypercapnia, the average firing rate of post-I (BötC) neurons is reduced. As such, late-E (pFRG) neurons reach their threshold for activation earlier in the expiratory phase (Fig. 9A), and the duration of late-E bursts extends over a longer interval at the end of expiration.

In Jenkin et al. (2017), inhibition of the KF during hypercapnia decreased the amplitude of post-I activity in the cVN. In the present model, the excitatory post-I (e) (BötC) population shapes the postinspiratory component of the cVN activity (Fig. 1). This population receives strong inhibition from aug-E neurons (BötC); this inhibition determines the phase duration of post-I (e) (BötC) activity and, hence, the phase duration of the postinspiratory component of cVN activity. The onset time of aug-E activity (BötC) in the respiratory cycle is determined by the inhibition that it receives from the inhibitory post-I neurons (BötC). This inhibition is gradually removed as post-I activity decrements and aug-E activity is eventually released. In the simulation of hypercapnia and KF inhibition, the average firing rate of post-I neurons (BötC) is decreased and aug-E (BötC) activity is recruited earlier in the expiratory phase (Fig. 9A; Fig. 10) compared with the hypercapnia simulation (Fig. 9B; Fig. 10). In this way, the phase duration of post-I (e) (BötC) and the postinspiratory component of the cVN activity is reduced through disinhibition of aug-E neurons.

Amplification of post-I inhibition abolishes AbN late-E activity. The effect of microinjections of gabazine in the KF was reproduced in the current extended model by increasing the KF drive to post-I (BötC) and early-I (BötC) neurons, and we refer to this manipulation as disinhibition of the KF. It is important to note that our model simulations reproduced the effects caused by the doses of gabazine used in the present experimental study, which did not disrupt the three-phase breathing pattern, and differ from results of another study that used higher concentrations of GABA_A receptor antagonists (Abdala et al. 2016). The simulation of hypercapnia and KF disinhibition (Fig. 8C; Fig. 9C) complements the simulation of hypercapnia and KF inhibition (Fig. 8A; Fig. 9A) and the

simulation of hypercapnia alone (control condition; Fig. 8B; Fig. 9B). In our simulations, the model reproduced the suppression in the AbN motoneuron output after KF disinhibition (Fig. 8C). We attributed the suppression of active expiration to the increase in the tonic KF drive to the inhibitory post-I neurons (BötC). The average firing rate of the post-I (BötC) population increased during simulation of hypercapnia and disinhibition of the KF (Fig. 9C) compared with the simulation of hypercapnia without perturbation to the KF drive (Fig. 9B). The increase in firing rate of the post-I population (BötC) led to an overall increase in inhibition of late-E neurons (pFRG) during expiration such that late-E activity (pFRG) could not be activated despite increased chemosensitive drive from the RTN.

The post-I (e) (BötC) population increased its firing duration (Fig. 9C). An increase in average firing rate of the post-I (BötC) population distributed more inhibition to its postsynaptic targets. This increase in inhibition is offset in the early-I population by the increase in tonic KF drive, but there is no mechanism to compensate for the increase in inhibition to aug-E (BötC) neurons. The onset time of the E2 burst of aug-E (BötC) neurons was delayed, and thus the duration of post-I (e) (BötC) activity increased (Fig. 9C; Fig. 10).

DISCUSSION

Active expiration emerges as a reflex mechanism to increase minute ventilation and support blood gas homeostasis in states of high metabolic demand (Jenkin and Milsom 2014; Lemes and Zoccal 2014). An important motor component of the active expiratory pattern is the development of high-amplitude bursts in abdominal expiratory motor activity, not seen in eupnea. Under hypercapnic conditions, these abdominal bursts are present during the late-E phase of the respiratory cycle, in association with reduced upper airway resistance and increased sympathetic outflow (Abdala et al. 2009; de Britto and Moraes 2017; Molkov et al. 2011). This evoked late-E discharge in AbN activity reported in the decerebrate *in situ* preparation resembles the pattern recorded in *in vivo* (more intact) preparations (Iizuka and Fregosi 2007; Moraes et al. 2013; Pagliardini et al. 2011), indicating that this pattern formation depends primarily on neural mechanisms within the brain stem. In the present study, we provide novel insights supporting a conditional inhibitory role of the KF neurons regulating the timing of abdominal late-E bursts in conditions of high chemosensory drive. We present modeling simulations, based on experimental data, elucidating possible interactions between the KF and the pFRG, through the BötC, which might help to explain, at least in part, the inhibitory effect of KF inputs on the threshold for activation of the expiratory oscillator.

The generation of active expiration has been attributed to a conditional expiratory oscillator located in the pFRG (Janczewski and Feldman 2006), whose activity is suggested to be defined by a balance between excitatory and inhibitory inputs (Marina et al. 2010; Molkov et al. 2010; Moraes et al. 2012; Pagliardini et al. 2011; Rubin et al. 2011). Under normoxic/eucapnic conditions, the expiratory neurons of the pFRG are tonically suppressed by inhibitory synapses (Pagliardini et al. 2011). During hypercapnia or hypoxia, this oscillator is activated because of increased excitation from central and peripheral chemoreceptors (Marina et al. 2010; Moraes et al. 2012)

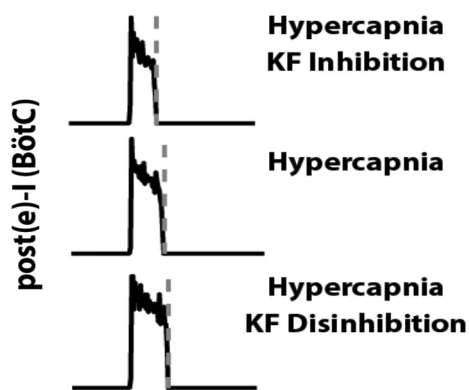


Fig. 10. Comparison of postinspiratory activity among 3 hypercapnia simulations. Activity of the post-I (e) (BötC) determines the postinspiratory component of the cVN burst. Vertical dashed line in each trace indicates the end of the postinspiratory burst.

and reduction in the inhibitory drive to the pFRG (Abdala et al. 2009; de Britto and Moraes 2017). Under eucapnic normoxic conditions, activation and disinhibition of the KF with micro-injections of glutamate and gabazine, respectively, did not modify abdominal activity. This finding agrees with previous studies demonstrating that baseline abdominal activity did not change after inhibition of the KF, despite significant modifications in phrenic and vagal motor outputs (Bautista and Dutschmann 2016; Jenkin et al. 2017). These data suggest that, under resting conditions, the KF inputs to the respiratory CPG are important for three-phase respiratory pattern formation, contributing to the inspiratory off-switch and the control of inspiratory-expiratory phase transition (Dutschmann et al. 2014), but do not influence the generation of baseline abdominal activity and the activity of pFRG expiratory neurons.

On the other hand, pharmacological manipulations of the KF during hypercapnia revealed that changes in KF drive to the respiratory CPG affect the emergence and timing of the AbN late-E activity in conditions of elevated chemosensitive drive. We previously demonstrated in rats that inhibition of the KF with isoguvacine reduced baseline post-I vagal activity and advanced the onset of late-E abdominal bursts in the expiratory phase (Jenkin et al. 2017). Here we report that KF disinhibition with low doses of gabazine (100 μ M) during hypercapnia generates a modest increase in baseline post-I activity in the vagus nerve but markedly attenuates the emergence of late-E bursts in the abdominal motor output. In these experiments, we sought to promote a moderate disinhibition of the KF by using lower doses of a GABA_A receptor antagonist [100 μ M gabazine vs. 5 mM bicuculline in Abdala et al. (2016)] to avoid excessive KF overactivity and the generation of exaggerated post-I bursts in vagus nerve activity associated with periods of apnea, as described previously (Abdala et al. 2016). These findings reveal a conditional inhibitory role of the KF that effectively controls the timing and generation of abdominal bursts during hypercapnia. Teppema et al. (1997) reported an increase in fos expression at the region of the KF after hypercapnia exposure. Interestingly, most hypercapnia-activated KF neurons that send projections to respiratory neurons in the lower brain stem and spinal cord are glutamatergic (Yokota et al. 2015). In light of this, we hypothesize that the KF impedes the emergence of late expiratory activity through an indirect inhibitory pathway that controls the pFRG neuronal activity. The recruitment of this KF-driven pathway during hypercapnia might be important for promoting phasic inhibition of expiratory neurons in the pFRG, then contributing to late-expiratory pattern formation. Interestingly, modifications in the strength of this pathway may modulate the active expiratory pattern, as seen during sleep-wake cycles (Andrews and Pagliardini 2015; Leirão et al. 2017).

We consider the possibility that the KF controls the threshold for activation of the late-E (pFRG) neuronal population and the emergence of late-E activity in the AbN through inhibition from post-I (BötC) neurons. This assumption was based on the following experimental observations: 1) projections from the KF to the other pontine and medullary regions that control respiratory function are predominantly excitatory (glutamatergic) (Geerling et al. 2017); 2) we found an inverse relationship between post-I and late-E motor activities (present study and Jenkin et al. 2017); 3) post-I neurons of the BötC are suggested as an important source of inhibition to the pFRG (Molkov et al.

2010); 4) the activity of post-I neurons in the BötC requires pontine drive (Smith et al., 2007); and 5) studies using retrograde labeling (Gang et al. 1995) and antidromic stimulation (Ezure and Tanaka 2006) suggest the existence of projections from the KF to the BötC region. This hypothesis was incorporated and tested in our model of respiratory CPG. In this model, the KF provided an excitatory drive to inhibitory post-I neurons in the BötC, which in turn inhibited late-E neurons in the pFRG. This KF-driven post-I population in the BötC also established inhibitory connections with inspiratory population in the pre-BötC. In model simulations, mild KF inhibition during hypercapnia led to suppression of post-I (BötC) activity, which reduced the threshold necessary for the activation of late-E (pFRG) neurons, thus advancing the breakthrough of late-E activity and prolonging its burst duration. In the simulation of mild KF disinhibition during hypercapnia, the enhanced post-I (BötC) activity did not decrement enough to release late-E (pFRG) activity. Hence, late-E bursts did not appear in the AbN. Therefore, our modeling simulations suggest a potential mechanism by which KF inputs may determine the intensity of post-I (BötC) discharge, which, in turn, finely controls the emergence of AbN late-E activity and its duration during hypercapnia. This theoretical mechanism still awaits experimental confirmation but parallels previous studies showing that more extreme reductions in the pontine drive to post-I (BötC) neurons, as seen in conditions of ischemia, generate late-E/post-I biphasic abdominal bursts (Abdala et al. 2009; Molkov et al. 2010; Rubin et al. 2011).

Previously, we investigated the role of phasic ponto-medullary interactions in models that included pulmonary feedback (Molkov et al. 2013; Rybak et al. 2004). Given these interactions, it is safe to assume that, qualitatively, the variation of excitability of pontine neurons would give rise to variation in the tonic drive to the populations they project to. Therefore, in the present study, for simplicity, we implemented the contributions of the pontine nuclei as a variable tonic excitatory drive. This allowed us to make some generic assumptions about the effect of the pharmacological manipulations delivered by isoguvacine and gabazine without addressing specific cell types in the pons. Those assumptions were that 1) there is a tonic pontine drive that is invariant in the face of these manipulations and 2) there is a tonic pontine drive that we attribute to the KF whose amplitude is subject to our manipulations. This simplification also allowed us to formulate a specific hypothesis for the role of KF input to the CPG in the regulation of the emergence of active expiration.

Previous studies demonstrated that the antagonism of GABA_A and glycinergic receptors in the pFRG generates abdominal late-E activity under normoxic and eucapnic conditions (de Britto and Moraes 2017; Molkov et al. 2010; Pagliardini et al. 2011). Our present model supports the hypothesis that late-E activity is markedly controlled by inhibitory inputs from the respiratory CPG. In our *in situ* experiments, we observed that KF inhibition did not evoke active expiration at rest (Jenkin et al. 2017). Although our microinjections may have not inhibited all neurons in the KF, these data suggest that other sources of inhibitory input to the pFRG may also contribute to tonic inhibition of the expiratory oscillator. These sources may include inhibitory projections from the nucleus of the solitary tract (Takakura et al. 2007).

In conclusion, our experimental data indicate that KF-driven inputs to the respiratory CPG control the presence and onset timing of AbN late-E bursts during exposure to high CO₂. Our model simulations propose that this inhibitory effect of the KF on hypercapnia-induced AbN activity is indirect and involves connections with post-I neurons of the BötC, which in turn inhibit expiratory neurons in the pFRG. Although the proposed model requires further anatomic and functional validation, our findings are relevant for exploring the mechanisms underpinning the generation of active expiration in conditions of chronic intermittent (Zoccal et al. 2008, 2009) or sustained (Moraes et al. 2014) hypoxia. In these experimental conditions, the emergence of late-E activity at rest is suggested to be associated with depressed post-I BötC activity (Moraes et al. 2014; Zoccal et al. 2008) and sensitization of chemosensitive neurons in the RTN (Molkov et al. 2011). Therefore, the hypoxia-induced reduction of the pontine drive to the medullary respiratory circuits, causing a reduction in excitability of the post-I (BötC) population, may promote active expiration in eucapnia by reducing the baseline expiratory inhibition in late-E. Moreover, hyperactivity of the KF neurons has been suggested as a mechanism that generates respiratory instabilities in the mouse model of Rett syndrome (Abdala et al. 2016). During central apneas in *Mecp2*-deficient mice, sustained expiratory activities are observed in the hypoglossal, vagus, and abdominal nerves (Abdala et al. 2010). This mouse model also exhibits reduced ventilatory responses to hypercapnia (Toward et al. 2013). Although our present model does not explain the generation of the respiratory phenotype seen in Rett syndrome, it certainly forms a platform from which to conceptualize the mechanisms responsible for the generation of central apneas and respiratory cycle irregularity in multiple disorders.

GRANTS

This study was supported by the National Institutes of Health (NIH) (Grants R01 AT-008632 and U01 EB-21960) and the São Paulo Research Foundation (FAPESP) (Grant 2013/17.251-6). This work utilized the computational resources of the NIH HPC Biowulf cluster (<https://hpc.nih.gov>).

DISCLOSURES

No conflicts of interest, financial or otherwise, are declared by the authors.

AUTHOR CONTRIBUTIONS

W.H.B., A.P.A., Y.I.M., and D.B.Z. conceived and designed research; W.H.B. and D.B.Z. performed experiments; W.H.B., A.P.A., Y.I.M., and D.B.Z. analyzed data; W.H.B., S.E.J., W.K.M., J.F.P., A.P.A., Y.I.M., and D.B.Z. interpreted results of experiments; W.H.B. and D.B.Z. prepared figures; W.H.B., A.P.A., Y.I.M., and D.B.Z. drafted manuscript; W.H.B., S.E.J., W.K.M., J.F.P., A.P.A., Y.I.M., and D.B.Z. edited and revised manuscript; W.H.B., S.E.J., W.K.M., J.F.P., A.P.A., Y.I.M., and D.B.Z. approved final version of manuscript.

REFERENCES

- Abbott SB, Stornetta RL, Coates MB, Guyenet PG. Phox2b-expressing neurons of the parafacial region regulate breathing rate, inspiration, and expiration in conscious rats. *J Neurosci* 31: 16410–16422, 2011. doi:10.1523/JNEUROSCI.3280-11.2011.
- Abdala AP, Dutschmann M, Bissonnette JM, Paton JF. Correction of respiratory disorders in a mouse model of Rett syndrome. *Proc Natl Acad Sci USA* 107: 18208–18213, 2010. doi:10.1073/pnas.1012104107.
- Abdala AP, Rybak IA, Smith JC, Paton JF. Abdominal expiratory activity in the rat brainstem-spinal cord in situ: patterns, origins and implications for respiratory rhythm generation. *J Physiol* 587: 3539–3559, 2009. doi:10.1113/jphysiol.2008.167502.
- Abdala AP, Toward MA, Dutschmann M, Bissonnette JM, Paton JF. Deficiency of GABAergic synaptic inhibition in the Kölliker-Fuse area underlies respiratory dysrhythmia in a mouse model of Rett syndrome. *J Physiol* 594: 223–237, 2016. doi:10.1113/JP270966.
- Anderson TM, Garcia AJ 3rd, Baertsch NA, Pollak J, Bloom JC, Wei AD, Rai KG, Ramirez JM. A novel excitatory network for the control of breathing. *Nature* 536: 76–80, 2016. doi:10.1038/nature18944.
- Andrews CG, Pagliardini S. Expiratory activation of abdominal muscle is associated with improved respiratory stability and an increase in minute ventilation in REM epochs of adult rats. *J Appl Physiol* (1985) 119: 968–974, 2015. doi:10.1152/japplphysiol.00420.2015.
- Barnett WH, Abdala AP, Paton JF, Rybak IA, Zoccal DB, Molkov YI. Chemoreception and neuroplasticity in respiratory circuits. *Exp Neurol* 287: 153–164, 2017. doi:10.1016/j.expneurol.2016.05.036.
- Bautista TG, Dutschmann M. Inhibition of the pontine Kölliker-Fuse nucleus abolishes eupneic inspiratory hypoglossal motor discharge in rat. *Neuroscience* 267: 22–29, 2014. doi:10.1016/j.neuroscience.2014.02.027.
- Bautista TG, Dutschmann M. The role of the Kölliker-Fuse nuclei in the determination of abdominal motor output in a perfused brainstem preparation of juvenile rat. *Respir Physiol Neurobiol* 226: 102–109, 2016. doi:10.1016/j.resp.2015.07.012.
- Bonis JM, Neumueller SE, Krause KL, Pan LG, Hodges MR, Forster HV. Contributions of the Kölliker-Fuse nucleus to coordination of breathing and swallowing. *Respir Physiol Neurobiol* 189: 10–21, 2013. doi:10.1016/j.resp.2013.06.003.
- de Britto AA, Moraes DJ. Non-chemosensitive parafacial neurons simultaneously regulate active expiration and airway patency under hypercapnia in rats. *J Physiol* 595: 2043–2064, 2017. doi:10.1113/JP273335.
- Dutschmann M, Dick TE. Pontine mechanisms of respiratory control. *Compr Physiol* 2: 2443–2469, 2012. doi:10.1002/cphy.c100015.
- Dutschmann M, Herbert H. The Kölliker-Fuse nucleus gates the postinspiratory phase of the respiratory cycle to control inspiratory off-switch and upper airway resistance in rat. *Eur J Neurosci* 24: 1071–1084, 2006. doi:10.1111/j.1460-9568.2006.04981.x.
- Dutschmann M, Jones SE, Subramanian HH, Stanic D, Bautista TG. The physiological significance of postinspiration in respiratory control. *Prog Brain Res* 212: 113–130, 2014. doi:10.1016/B978-0-444-63488-7.00007-0.
- Ezure K, Tanaka I. Distribution and medullary projection of respiratory neurons in the dorsolateral pons of the rat. *Neuroscience* 141: 1011–1023, 2006. doi:10.1016/j.neuroscience.2006.04.020.
- Gang S, Sato Y, Kohama I, Aoki M. Afferent projections to the Bötzing complex from the upper cervical cord and other respiratory related structures in the brainstem in cats: retrograde WGA-HRP tracing. *J Auton Nerv Syst* 56: 1–7, 1995. doi:10.1016/0165-1838(95)00049-X.
- Geerling JC, Yokota S, Rukhadze I, Roe D, Chamberlin NL. Kölliker-Fuse GABAergic and glutamatergic neurons project to distinct targets. *J Comp Neurol* 525: 1844–1860, 2017. doi:10.1002/cne.24164.
- Guthmann A, Fritschy JM, Ottersen OP, Torp R, Herbert H. GABA, GABA transporters, GABA_A receptor subunits, and GAD mRNAs in the rat parabrachial and Kölliker-Fuse nuclei. *J Comp Neurol* 400: 229–243, 1998. doi:10.1002/(SICI)1096-9861(19981019)400:2<229::AID-CNE5>3.0.CO;2-B.
- Harris MB, Milsom WK. Apneusis follows disruption of NMDA-type glutamate receptors in vagotomized ground squirrels. *Respir Physiol Neurobiol* 134: 191–207, 2003. doi:10.1016/S1569-9048(02)00223-9.
- Iizuka M, Fregosi RF. Influence of hypercapnic acidosis and hypoxia on abdominal expiratory nerve activity in the rat. *Respir Physiol Neurobiol* 157: 196–205, 2007. doi:10.1016/j.resp.2007.01.004.
- Janczewski WA, Feldman JL. Distinct rhythm generators for inspiration and expiration in the juvenile rat. *J Physiol* 570: 407–420, 2006. doi:10.1113/jphysiol.2005.098848.
- Jenkin SE, Milsom WK. Expiration: breathing's other face. *Prog Brain Res* 212: 131–147, 2014. doi:10.1016/B978-0-444-63488-7.00008-2.
- Jenkin SE, Milsom WK, Zoccal DB. The Kölliker-Fuse nucleus acts as a timekeeper for late-expiratory abdominal activity. *Neuroscience* 348: 63–72, 2017. doi:10.1016/j.neuroscience.2017.01.050.
- Leirão IP, Silva CA Jr, Gargaglioni LH, da Silva GSF. Hypercapnia-induced active expiration increases in sleep and enhances ventilation in anaesthetized rats. *J Physiol*, 2017. doi:10.1113/JP274726.
- Lemes EV, Zoccal DB. Vagal afferent control of abdominal expiratory activity in response to hypoxia and hypercapnia in rats. *Respir Physiol Neurobiol* 203: 90–97, 2014. doi:10.1016/j.resp.2014.08.011.

- Levitt ES, Abdala AP, Paton JF, Bissonnette JM, Williams JT.** μ Opioid receptor activation hyperpolarizes respiratory-controlling Kölliker-Fuse neurons and suppresses post-inspiratory drive. *J Physiol* 593: 4453–4469, 2015. doi:10.1113/JP270822.
- Lumsden T.** Observations on the respiratory centres in the cat. *J Physiol* 57: 153–160, 1923. doi:10.1113/jphysiol.1923.sp002052.
- Mandel DA, Schreihofer AM.** Modulation of the sympathetic response to acute hypoxia by the caudal ventrolateral medulla in rats. *J Physiol* 587: 461–475, 2009. doi:10.1113/jphysiol.2008.161760.
- Marina N, Abdala AP, Trapp S, Li A, Nattie EE, Hewinson J, Smith JC, Paton JF, Gourine AV.** Essential role of Phox2b-expressing ventrolateral brainstem neurons in the chemosensory control of inspiration and expiration. *J Neurosci* 30: 12466–12473, 2010. doi:10.1523/JNEUROSCI.3141-10.2010.
- McCormick DA, Pape HC.** Properties of a hyperpolarization-activated cation current and its role in rhythmic oscillation in thalamic relay neurones. *J Physiol* 431: 291–318, 1990. doi:10.1113/jphysiol.1990.sp018331.
- Mifflin SW.** Arterial chemoreceptor input to respiratory hypoglossal motoneurons. *J Appl Physiol* (1985) 69: 700–709, 1990. doi:10.1152/jappl.1990.69.2.700.
- Molkov YI, Abdala AP, Bacak BJ, Smith JC, Paton JF, Rybak IA.** Late-expiratory activity: emergence and interactions with the respiratory CpG. *J Neurophysiol* 104: 2713–2729, 2010. doi:10.1152/jn.00334.2010.
- Molkov YI, Bacak BJ, Dick TE, Rybak IA.** Control of breathing by interacting pontine and pulmonary feedback loops. *Front Neural Circuits* 7: 16, 2013. doi:10.3389/fncir.2013.00016.
- Molkov YI, Shevtsova NA, Park C, Ben-Tal A, Smith JC, Rubin JE, Rybak IA.** A closed-loop model of the respiratory system: focus on hypercapnia and active expiration. *PLoS One* 9: e109894, 2014. doi:10.1371/journal.pone.0109894.
- Molkov YI, Zoccal DB, Moraes DJ, Paton JF, Machado BH, Rybak IA.** Intermittent hypoxia-induced sensitization of central chemoreceptors contributes to sympathetic nerve activity during late expiration in rats. *J Neurophysiol* 105: 3080–3091, 2011. doi:10.1152/jn.00070.2011.
- Moraes DJ, Bonagamba LG, Costa KM, Costa-Silva JH, Zoccal DB, Machado BH.** Short-term sustained hypoxia induces changes in the coupling of sympathetic and respiratory activities in rats. *J Physiol* 592: 2013–2033, 2014. doi:10.1113/jphysiol.2013.262212.
- Moraes DJ, da Silva MP, Bonagamba LG, Mecawi AS, Zoccal DB, Antunes-Rodrigues J, Varanda WA, Machado BH.** Electrophysiological properties of rostral ventrolateral medulla presympathetic neurons modulated by the respiratory network in rats. *J Neurosci* 33: 19223–19237, 2013. doi:10.1523/JNEUROSCI.3041-13.2013.
- Moraes DJ, Dias MB, Cavalcanti-Kwiatkoski R, Machado BH, Zoccal DB.** Contribution of the retrotrapezoid nucleus/parafacial respiratory region to the expiratory-sympathetic coupling in response to peripheral chemoreflex in rats. *J Neurophysiol* 108: 882–890, 2012. doi:10.1152/jn.00193.2012.
- Moreira TS, Takakura AC, Colombari E, West GH, Guyenet PG.** Inhibitory input from slowly adapting lung stretch receptors to retrotrapezoid nucleus chemoreceptors. *J Physiol* 580: 285–300, 2007. doi:10.1113/jphysiol.2006.125336.
- Morrison SF, Cravo SL, Wilfehrt HM.** Pontine lesions produce apneusis in the rat. *Brain Res* 652: 83–86, 1994. doi:10.1016/0006-8993(94)90320-4.
- Mörschel M, Dutschmann M.** Pontine respiratory activity involved in inspiratory/expiratory phase transition. *Philos Trans R Soc Lond B Biol Sci* 364: 2517–2526, 2009. doi:10.1098/rstb.2009.0074.
- Orem J, Trotter RH.** Postinspiratory neuronal activities during behavioral control, sleep, and wakefulness. *J Appl Physiol* (1985) 72: 2369–2377, 1992. doi:10.1152/jappl.1992.72.6.2369.
- Pagliardini S, Janczewski WA, Tan W, Dickson CT, Deisseroth K, Feldman JL.** Active expiration induced by excitation of ventral medulla in adult anesthetized rats. *J Neurosci* 31: 2895–2905, 2011. doi:10.1523/JNEUROSCI.5338-10.2011.
- Paton JF.** The ventral medullary respiratory network of the mature mouse studied in a working heart-brainstem preparation. *J Physiol* 493: 819–831, 1996. doi:10.1113/jphysiol.1996.sp021425.
- Paxinos G, Watson C.** *The Rat Brain in Stereotaxic Coordinates*. Amsterdam: Academic/Elsevier, 2007.
- Rosin DL, Chang DA, Guyenet PG.** Afferent and efferent connections of the rat retrotrapezoid nucleus. *J Comp Neurol* 499: 64–89, 2006. doi:10.1002/cne.21105.
- Rubin JE, Bacak BJ, Molkov YI, Shevtsova NA, Smith JC, Rybak IA.** Interacting oscillations in neural control of breathing: modeling and qualitative analysis. *J Comput Neurosci* 30: 607–632, 2011. doi:10.1007/s10827-010-0281-0.
- Rybak IA, Abdala AP, Markin SN, Paton JF, Smith JC.** Spatial organization and state-dependent mechanisms for respiratory rhythm and pattern generation. *Prog Brain Res* 165: 201–220, 2007. doi:10.1016/S0079-6123(06)65013-9.
- Rybak IA, Paton JF, Schwaber JS.** Modeling neural mechanisms for genesis of respiratory rhythm and pattern. I. Models of respiratory neurons. *J Neurophysiol* 77: 1994–2006, 1997. doi:10.1152/jn.1997.77.4.1994.
- Rybak IA, Shevtsova NA, Paton JF, Dick TE, St-John WM, Mörschel M, Dutschmann M.** Modeling the ponto-medullary respiratory network. *Respir Physiol Neurobiol* 143: 307–319, 2004. doi:10.1016/j.resp.2004.03.020.
- Silva JN, Lucena EV, Silva TM, Damasceno RS, Takakura AC, Moreira TS.** Inhibition of the pontine Kölliker-Fuse nucleus reduces genioglossal activity elicited by stimulation of the retrotrapezoid chemoreceptor neurons. *Neuroscience* 328: 9–21, 2016a. doi:10.1016/j.neuroscience.2016.04.028.
- Silva JN, Tanabe FM, Moreira TS, Takakura AC.** Neuroanatomical and physiological evidence that the retrotrapezoid nucleus/parafacial region regulates expiration in adult rats. *Respir Physiol Neurobiol* 227: 9–22, 2016b. doi:10.1016/j.resp.2016.02.005.
- Smith JC, Abdala AP, Koizumi H, Rybak IA, Paton JF.** Spatial and functional architecture of the mammalian brain stem respiratory network: a hierarchy of three oscillatory mechanisms. *J Neurophysiol* 98: 3370–3387, 2007. doi:10.1152/jn.00985.2007.
- Smith JC, Ellenberger HH, Ballanyi K, Richter DW, Feldman JL.** Pre-Bötzinger complex: a brainstem region that may generate respiratory rhythm in mammals. *Science* 254: 726–729, 1991. doi:10.1126/science.1683005.
- St-John WM, Paton JF.** Role of pontile mechanisms in the neurogenesis of apnea. *Respir Physiol Neurobiol* 143: 321–332, 2004. doi:10.1016/j.resp.2004.05.010.
- Takakura AC, Moreira TS, West GH, Gwilt JM, Colombari E, Stornetta RL, Guyenet PG.** GABAergic pump cells of solitary tract nucleus innervate retrotrapezoid nucleus chemoreceptors. *J Neurophysiol* 98: 374–381, 2007. doi:10.1152/jn.00322.2007.
- Teppema LJ, Veening JG, Kranenburg A, Dahan A, Berkenbosch A, Olivier C.** Expression of c-fos in the rat brainstem after exposure to hypoxia and to normoxic and hyperoxic hypercapnia. *J Comp Neurol* 388: 169–190, 1997. doi:10.1002/(SICI)1096-9861(19971117)388:2<169::AID-CNE1>3.0.CO;2-#.
- Toward MA, Abdala AP, Knopp SJ, Paton JF, Bissonnette JM.** Increasing brain serotonin corrects CO₂ chemosensitivity in methyl-CpG-binding protein 2 (Mecp2)-deficient mice. *Exp Physiol* 98: 842–849, 2013. doi:10.1113/expphysiol.2012.069872.
- Yokota S, Kaur S, VanderHorst VG, Saper CB, Chamberlin NL.** Respiratory-related outputs of glutamatergic, hypercapnia-responsive parabrachial neurons in mice. *J Comp Neurol* 523: 907–920, 2015. doi:10.1002/cne.23720.
- Zoccal DB, Bonagamba LG, Paton JF, Machado BH.** Sympathetic-mediated hypertension of awake juvenile rats submitted to chronic intermittent hypoxia is not linked to baroreflex dysfunction. *Exp Physiol* 94: 972–983, 2009. doi:10.1113/expphysiol.2009.048306.
- Zoccal DB, Simms AE, Bonagamba LG, Braga VA, Pickering AE, Paton JF, Machado BH.** Increased sympathetic outflow in juvenile rats submitted to chronic intermittent hypoxia correlates with enhanced expiratory activity. *J Physiol* 586: 3253–3265, 2008. doi:10.1113/jphysiol.2008.154187.